**Carlos M. Xisto**[1]
Division of Fluid Dynamics,
Department of Applied Mechanics,
Chalmers University of Technology,
Gothenburg SE-41296, Sweden
e-mail: carlos.xisto@chalmers.se

**José C. Páscoa**
Departamento de Engenharia Electromecânica,
Universidade da Beira Interior,
Covilhã 6200, Portugal
e-mail: pascoa@ubi.pt

**Michele Trancossi**
Department of Engineering and Mathematics,
Sheffield Hallam University,
Sheffield, South Yorkshire S1 1WB, UK
e-mail: m.trancossi@shu.ac.uk

# Geometrical Parameters Influencing the Aerodynamic Efficiency of a Small-Scale Self-Pitch High-Solidity VAWT

*In this paper, four key design parameters with a strong influence on the performance of a high-solidity variable pitch vertical axis wind turbine (VAWT) operating at low tip-speed-ratio (TSR) are addressed. To this aim, a numerical approach, based on a finite-volume discretization of two-dimensional (2D) unsteady Reynolds-averaged Navier–Stokes (URANS) equations, on a multiple sliding mesh, is proposed and validated against experimental data. The self-pitch VAWT design is based on a straight-blade Darrieus wind turbine with blades that are allowed to pitch around a feathering axis, which is also parallel to the axis of rotation. The pitch angle amplitude and periodic variation are dynamically controlled by a four-bar linkage system. We only consider the efficiency at low and intermediate TSR; therefore, the pitch amplitude is chosen to be a sinusoidal function with a considerable amplitude. The results of this parametric analysis will contribute to define the guidelines for building a full-size prototype of a small-scale wind turbine of increased efficiency.* [DOI: 10.1115/1.4032794]

## 1 Introduction

VAWTs can be classified as being drag-based or lift-based devices. Lift-based, or Darrieus, wind turbines are composed of a set of straight or curved troposkein-shaped airfoils. These generate power by converting the tangential component of lift into positive torque. The curved troposkein-shaped blade design was proposed to reduce the structural centrifugal loads. The straight-blade rotor, also known as H-rotor, is more sensible to the centrifugal loads but have a more useful area of operation, since the entire span of blade length is operating at the same tip speed. Nevertheless, these turbines are limited to the amount of energy that they can extract from the wind, which is normally lower than the one gathered by horizontal axis wind turbines (HAWTs). Still, there are several aspects that might enable the introduction of VAWT technology in the energy production market [1]. One clear advantage of VAWTs over HAWTs is that they are omnidirectional, i.e., they accept wind from any directions without the need of a yaw system to redirect the turbine toward the wind. This feature is quite useful in regions where unstable and high turbulent wind can cause significant problems for HAWTs [2]. In a VAWT, the generator system is located on the ground level, whereas in an HAWT, it needs to be fitted on the top of the tower, which increases the initial capital cost since the HAWT supporting structure is heavier and expensive. The operation costs are also expected to be higher in an HAWT since the components are more inaccessible for maintenance. Another inherent advantage is that H-rotors are composed of a set of symmetric airfoils, which are cheaper to manufacture. On the other side, the blades of HAWTs are much more complex, since they require taper, twist, and varying airfoil section in the spanwise direction. Still, there is a big gap between the efficiency of an HAWT and a VAWT in ideal wind conditions. In order to close that gap, a new technology of VAWT that can have a superior or equivalent efficiency than HAWT is required. We propose a concept of a dynamic self-pitch VAWT. There are several aspects, in which a variable pitch design can improve when compared with classical VAWTs and HAWTs, see Ref. [3] for more details.

In this paper, a small-scale, self-pitch, high-solidity VAWT is proposed for microelectricity generation in urban environment. The turbine is designed to operate at low and intermediate TSRs ($0.5 < \lambda < 1.5$) for aerodynamic noise attenuation. Noise in a wind turbine is mainly related to the blades tip-speed velocity and to the drive train components. VAWTs usually produce less aerodynamic noise since they operate at lower tip speeds than their horizontal counterparts, which are normally designed for much higher TSRs [2].

In the proposed system, the rotating blades are allowed to pitch around a feathering axis that is parallel to the axis of rotation. The pitch schedule and amplitude are controlled by a four-bar linkage type mechanism, see Fig. 1(*a*) [4], which is very similar to the Voith–Schneider wind turbine [5]. While using this system, it is possible to improve the azimuthal load distribution and energy conversion at low and intermediate $\lambda$. A pure straight-blade Darrieus turbine is normally composed of classic symmetric blade section profiles, these being usually designed to operate at small angles of attack ($\alpha$). If a critical $\alpha$ is achieved, the flow separates from the low pressure surface of the airfoil and the blade experiences stall. In a conventional fixed pitch VAWT, each blade experiences a periodic variation of $\alpha$, which has contributions from the incoming wind and rotational speeds, see Fig. 1(*b*). At high values of $\lambda$, the amplitude of $\alpha$ variation decreases and, as $V_t \gg V_{\text{wind}}$, the variation is almost negligible. Conversely, at intermediate $\lambda$, due to a large cyclic variation of $\alpha$, the blades on the rear half (with respect to wind direction, $\Psi = 270\,\text{deg}$) experience stall. At low $\lambda$, this effect is even more severe, consequently the turbine produces none or very low torque and loses the ability to self-start. With the proposed concept, a pitching schedule for the blades is defined as a function of their position in the rotating cycle. The oscillating movement of the blades minimizes the variation of the angle of attack, thus reducing stall effects in the rear half of the rotor for low and intermediate $\lambda$ values. For low $\lambda$, the blades could even be orientated to act as more efficient drag devices allowing to produce enough torque to start the turbine [6].

[1]Corresponding author.

Contributed by the Solar Energy Division of ASME for publication in the Journal of Solar Energy Engineering: Including Wind Energy and Building Energy Conservation. Manuscript received April 16, 2015; final manuscript received February 12, 2016; published online March 9, 2016. Assoc. Editor: Yves Gagnon.

 Copyright © 2016 by ASME 

Downloaded From: http://solarenergyengineering.asmedigitalcollection.asme.org/ on 03/09/2016 Terms of Use: http://www.asme.org/about-asme/terms-of-use

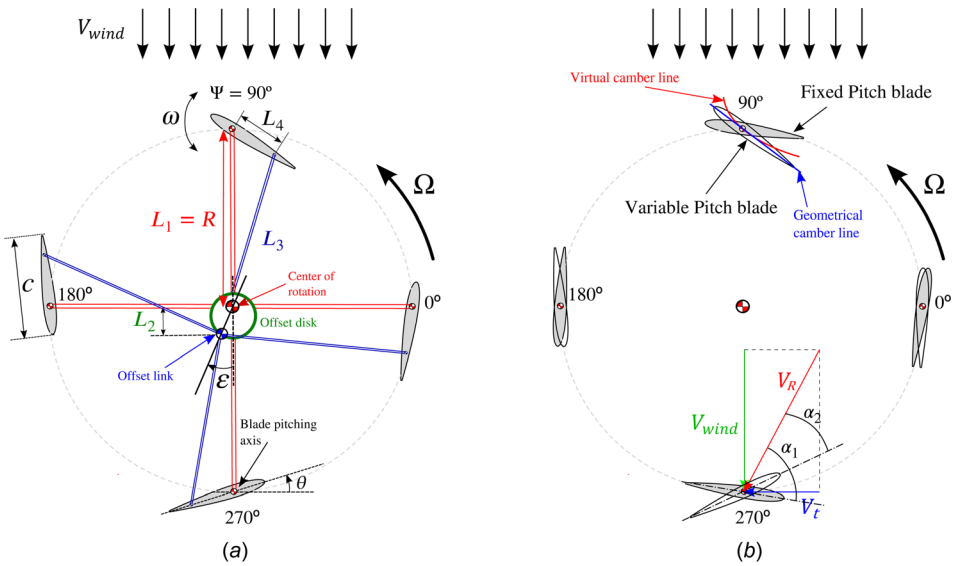


**Fig. 1 (*a*) Variable pitch VAWT with a four-bar linkage pitching system and (*b*) comparison between the velocity vectors at low TSR between a variable and fixed pitch VAWT. $V_t = \Omega R$ is the tip-speed velocity, and $V_R = \sqrt{V_{\text{wind}}^2 + V_t^2}$ is the resultant velocity on the blade. One can observe that, in the backward region of the VAWT ($\Psi = 270$ deg), the angle of attack, $\alpha$, is higher for the fixed pitch VAWT ($\alpha_1 > \alpha_2$).**

The power coefficient, $C_P$, which describes how much energy is possible to extract from the wind, is normally used to estimate the efficiency of wind turbines. HAWTs normally reach values of $C_P = 0.4$ to $C_P = 0.45$ [7]. In VAWTs, $C_P$ values of 0.4–0.43 were obtained 20 yrs ago [1] when many researchers proved, experimentally and analytically, that VAWTs can reach comparable performance levels to their horizontal axis counterparts. There are several aspects that could affect the performance of a wind turbine, namely, the design of an optimized airfoil [8], the modification of rotor solidity [7,9], or the inclusion of a variable pitch mechanism [10]; a more comprehensive VAWT parametric study can be found in Ref. [11] and a revision of VAWTs technology is given in Ref. [12]. In this paper, several of these geometrical parameters are analyzed in a variable pitch VAWT.

In Sec. 1.1, the pitch mechanism and the equations that express the oscillating motion of the blades are briefly presented. Afterward, in Sec. 2, the 2D numerical method is presented and validated with the available experimental data. The influence of the geometrical parameters is analyzed in Sec. 3, and the optimized design is compared with a fixed pitch VAWT in Sec. 4.

**1.1 Variable Pitch VAWT for Improved Aerodynamic Efficiency.** The experience gained and the recent developments on cyclogyros for aeronautics will be incorporated in this work to solve the problems of variable pitch vertical turbines. Through this cross-fertilization we propose, as a first approach, the pitching mechanism as shown in Fig. 1(*a*) [4]. It consists of three fixed lengths, $L_1$, $L_3$, and $L_4$, and it is controlled by the length and orientation of $L_2$. In the proposed design, the $L_1$ bar is equal to the rotor radius and is connected to the blade in the respective pitching axis. The $L_3$ bar is connected to the other end of the blade, and the distance between these two connections is $L_4$. All the links between the bars are free to rotate. Such mechanism allows for a cyclic pitching of the blades as they follow the path of rotation.

The dynamic pitching provided by the four-bar linkage mechanism is expressed by the following equations [13]:

$$\theta = \frac{\pi}{2} - \sin^{-1}\left[\frac{L_2}{a}\cos(\Psi + \varepsilon)\right] - \cos^{-1}\left[\frac{a^2 + L_4^2 - L_3^2}{2aL_4}\right] \tag{1}$$

where

$$a^2 = L_2^2 + R^2 - 2L_2R\cos\left(\Psi + \varepsilon + \frac{\pi}{2}\right) \tag{2}$$

The pitch angular speed is given by the time derivative of $\theta$

$$\omega = \frac{d\theta}{\mathrm{d}t} = \frac{d\theta}{d\Psi}\cdot\frac{d\Psi}{dt} = \frac{d\theta}{d\Psi}\cdot\Omega \tag{3}$$

This mechanism, which has proved well for cyclogyros used in aeronautical propulsion [13–18], is simple, reliable, and has the ability to self-adjust the turbine dynamics as a function of the rotating speed of the rotor and also on the direction and magnitude of the incoming wind. It is noted that the system kinematics also allows for an asymmetric pitching schedule of the blades, which could be beneficial since the frontal area of the rotor operates at a different angle of attack than the rear region. However, an increase in power penalty due to the friction losses as well the increasing possibility of system failure are anticipated consequences of adding more moving parts into the VAWT. Further, the pitching system needs to be aware of the wind conditions (direction and intensity) and rotational speed of the rotor. A set of sensors are therefore required and an intelligent control system needs to be devised, in order to assert the optimal rotor operational conditions that meet both aerodynamic efficiency and system structural integrity.

## 2 Numerical Method and Validation

The numerical work was performed with ANSYS FLUENT [19]. The numerical methodology is based on a finite-volume implementation of the incompressible, URANS equations on 2D hybrid grids. For simulating the rotational motion of the rotor, as well as the oscillating motion of the blades, a sliding-mesh method is used. The assumption of incompressible flow is justified on the basis of the maximum velocities involved. For coupling the dependent variables that compose the incompressible Navier–Stokes equations, a pressure-based coupled algorithm is used, which allows performing unsteady computations with a



Downloaded From: http://solarenergyengineering.asmedigitalcollection.asme.org/ on 03/09/2016 Terms of Use: http://www.asme.org/about-asme/terms-of-use

**Table 1 Numerical framework used in this paper**

| Solver | Pressure-based coupled solver; 2D; double-precision; sliding–mesh; URANS |
|---|---|
| Boundary conditions | Viscous wall (no-slip); uniform flow velocity inlet/outlet; $I = 5\%$ ; $l = 0.02c$ |
| Fluid type | Incompressible air |
| Spatial discretization | Second-order linear upwind; central-differences |
| Time discretization | Second-order implicit |
| Turbulence modeling ($y^+ < 1$) | $k$–$\omega$ SST/ Spalart–Allmaras |
| Grid size (IAT21) | 300,000 cells (grid 0); 600,000 cells (grid 1) |

Courant number of order 100 within each time-step. The remaining specifications of the numerical method, which will be used throughout this paper, are described in Table 1.

We start by validating the numerical model with the available experimental data. To this end, data for a cyclogyro of similar dimensions as the wind turbine, operating in propulsion mode ($V_{\text{wind}} = 0$), are used. This configuration, here denominated IAT21-L3 rotor, was analyzed as a part of an European research project, which aimed to develop the cyclogyro technology as a mean of propulsion for small and medium size aircraft [13,18,20–23]. It is obvious that the results obtained for the IAT21-L3 rotor do not faithfully represent the features of a VAWT, since in propulsion mode energy is being provided and not extracted from the flow. Nevertheless, the IAT21-L3 rotor comprises similar aerodynamic features that will allow us to validate the CFD model in terms of relative unsteady blade flows. Moreover, other authors have employed similar numerical models for studying the flow on classical VAWT [24,25], which indicates that the current numerical framework can be considered satisfactory for analyzing the flow in the proposed design. If a more detailed description of the flow is to be achieved, e.g., simulation of dynamic stall [26–28], the usage of detached eddy simulation or large-eddy simulation models is required.

The IAT21-L3 rotor is composed of six NACA0016 blades with a chord and span equal to $c = 0.3$ m and $S = 2R$ m, respectively, the rotor radius is equal to $R = 0.5$ m. The pitching axis is located at 35% of the chord length, and the distance between the pitching axis and the control rod is $L_4 = 0.120$ m. The periodic pitching schedule varies from $\theta = +36$ deg, in the top section of the rotor ($\Psi = 90$ deg), to $\theta = -39$ deg in the bottom section of the rotor ($\Psi = 270$ deg), resulting in an asymmetric pitching profile. This blade pitch angle variation is described by Eq. (1), and the angular velocity, $\omega$, of the oscillating blades is given by Eq. (3). The length of the control rod ($L_3 = 0.61$ m), the magnitude of eccentricity ($L_2 = 0.073$ m), and the phase angle of eccentricity ($\varepsilon = 0$ deg) were defined in order to obtain the desired pitching profile.

Figure 2 shows the numerical domain and boundary conditions, together with a close-up of the rotor and blade ($\Psi = 120$ deg) computational grids. The overall domain comprises three circular zones, which are separated by sliding-mesh interfaces. The first zone is the so-called "environment" that is fully covered by a stationary ($\Omega = 0$) unstructured grid; the second zone is the "rotor" that is also covered by an unstructured grid, but is rotating in the counterclockwise direction with a rotating speed $\Omega$; and finally, the third zone is the "blade" domain, which is composed of an hybrid grid comprising a fully structured O-type mesh in the boundary layer region, in order to comply with $y^+ < 1$, and a fully unstructured grid in the remaining domain. Each blade domain is centered in the pitching axis and prescribes an oscillating motion, $\omega$, given by Eq. (3). The boundary conditions are specified in the following way: for the validation test case, the outer circle BC works as an outlet, where the atmospheric pressure is specified; for the VAWT test cases, a velocity $U_{\text{wind}}$ is imposed together with a turbulence intensity, $I$, of 5%, which is a typical value for wind and a turbulence length scale of $l = 0.02\,c$ [19]. It is noted that in the Spalart–Allmaras (SA) turbulence model there is no significant term that provides a decay in turbulence intensity from the freestream boundary until the rotor [29], therefore for such a model a value of $I = 5\%$ on the rotor is also expected.

The results are obtained for several rotating speeds, $100 < \Omega < 1000$, which means that the chord-based Reynolds number is in the range of $12{,}560 < \text{Re}_c < 1{,}256{,}600$. For each value of $\Omega$, a total of 20 rotations are computed, but a time-converged periodic solution is obtained after ten revolutions. Therefore, thrust and power are presented in terms of time-average data obtained for the last ten rotations of each $\Omega$. For the VAWT test case, in Sec. 3, a periodic solution is obtained after the first two rotations, in that case only the last three revolutions of a total of five were used for obtaining the time-average values of $C_P$. The time-step is defined so as to obtain a rotor azimuthal displacement of $1/2$ deg per time-step [25].

Figure 3 shows a comparison between the numerical results and the experimental data. It is noted that thrust and power vary with the square and cube of rotation speed, respectively. In Fig. 3($a$), the results obtained for the time-averaged variation of thrust with rotation speed are compared with the experiments. The numerical results are also compared with each other in terms of turbulence model (SA, $k$–$\omega$ SST) and grid refinement (grid 0 and grid 1). One can observe that both turbulence models predict the same trend, and that the results do not significantly change as the number of grid points is increased. It is noted that this is a 2D model

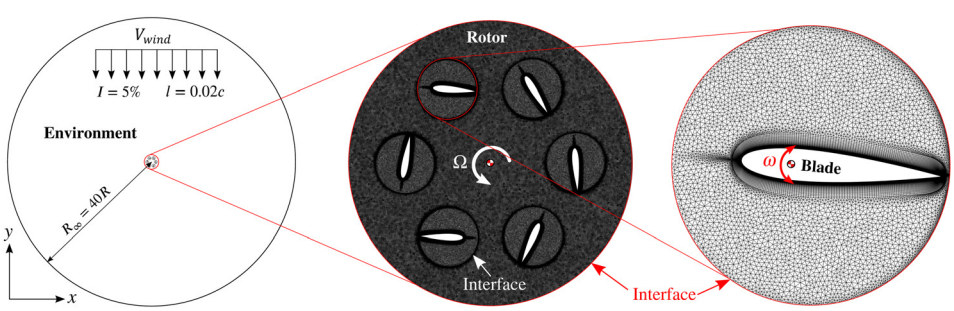


**Fig. 2 Two-dimensional numerical domain used for computing the IAT21-L3 rotor test case, a close-up of the rotor and blade grid is also displayed. The grid is composed by three circular zones, which are separated by sliding-mesh interfaces. The same numerical configuration and boundary conditions are used throughout this paper.**



Downloaded From: http://solarenergyengineering.asmedigitalcollection.asme.org/ on 03/09/2016 Terms of Use: http://www.asme.org/about-asme/terms-of-use

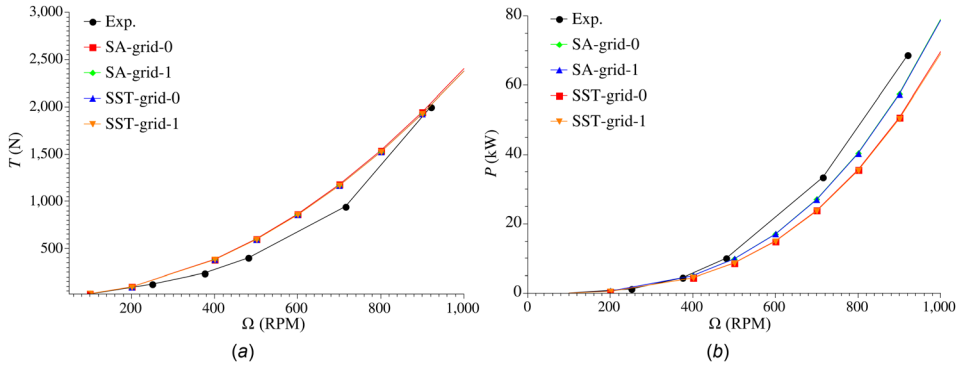


**Fig. 3 The results obtained for the validation test case in $\log_{10}-\log_{10}$ plots: (*a*) variation of thrust with rotational speed and (*b*) variation of power with rotational speed**

**Table 2 Rotor dimensions and parameters that were analyzed for the proposed VAWT design. Four parameters were computed: the airfoil thickness, the number of blades, the chord-to-radius ratio, and the location of the pitching axis, in terms of percentage of chord length.**

| Rotor dimensions | | Parameter | Variable |
|---|---|---|---|
| Span, $S$ | 1 m | NACA profile | 0006/0010/0015/0018 |
| Radius, $R$ | 0.5 m | No. of blades, $N$ | 2/3/4/6 |
| Pitch amplitude, $\theta_0$ | 30 deg | Chord, $c$ (m) | 0.125/0.25/0.375 |
| Rotational speed, $\Omega$ | 100 rpm | PA location ($x'/c$) | 0.125/0.25/0.35/0.5 |

and that the 3D losses are being neglected, which could explain the discrepancy between the experimental data and CFD results in some plot regions. Figure 3(*b*) shows the variation of power with rotational speed. Here, the comparison between the experiments and CFD shows a better agreement, once again the results do not significantly change with the refinement of the grid. However, in the prediction of power consumption, the SA turbulence model provides a better answer (the range of the numerical error is slightly lower than 10%) than the $k$–$\omega$ SST model. These are indicators that the results obtained with grid 0 are satisfactory in terms of grid refinement, and that the SA model could be used for the remaining part of this paper.

## 3 Analysis of 2D Geometrical Parameters

In this section, four geometrical parameters influencing the aerodynamic efficiency of a small-scale high-solidity VAWT, at low TSRs, are analyzed. We start by analyzing the influence of the airfoil thickness, afterward in Sec. 3.2, the effect of increasing the number of blades is assessed in a $C_P$ versus $\lambda$ plot. The chord-to-radius ratio and the pitching axis location are analyzed in Secs. 3.3 and 3.4, respectively. The rotor dimensions selected for the analysis are listed in Table 2. The rotor diameter and span are equal to 1 m, and the pitch angle amplitude is fixed between $+30$ deg and $-30$ deg. Such an high value for the amplitude, $\theta$, was chosen since for the lower TSRs, $\lambda < 1$, a higher pitching angle will give a lower variation of $\alpha$. This is illustrated in Fig. 1(*b*), where $\alpha_2$ is reduced with an increasing $\theta$. This will no longer be true for the intermediate, $\lambda = 1$, and higher, $\lambda > 1$, TSRs, since the variation of $\alpha$ decreases with an increasing $\lambda$. Therefore, an optimum $\theta$ will exist for a given $\lambda$, and normally $\theta$ should be increased as we decrease $\lambda$. For the parametric analysis, a sinusoidal pitch angle equation was used to described the oscillatory movement of the blades

$$\theta = \theta_0 \sin(\Omega t + \Psi_0) \tag{4}$$

The time derivative of Eq. (4) provides the angular pitching velocity of the blades

$$\omega = \dot{\theta} = \theta_0 \Omega \cos(\Omega t + \Psi_0) \tag{5}$$

where $\theta_0 = 30$ deg is the pitch amplitude, and $\Psi_0$ is the initial blade position. The rotor rotates counterclockwise and for the entire simulation, the rotational speed is fixed, $\Omega = 10.47$ rad/s (100 rpm). Therefore, in order to vary the TSR

$$\lambda = \frac{V_t}{V_{\text{wind}}} \tag{6}$$

only the wind velocity $V_{\text{wind}}$ varies. In Eq. (6), $V_t = \Omega R$ is the blade tip velocity, which is kept constant for the entire range of $\lambda$. In Secs. 3.1–3.4, the aerodynamic efficiency of the rotor is expressed in terms of power coefficient

$$C_P = \frac{P}{0.5\,\rho\,A\,V_{\text{wind}}^3} \tag{7}$$

variation with $\lambda$. The power coefficient relates the power extracted from the wind, $P = M\Omega$, with the total power contained in the wind $P_{\text{wind}} = 0.5\,\rho\,A\,V_{\text{wind}}^3$, where $\rho$ is the density of air, $A = 2RS$ is the rotor disk area, and $M$ is the torque.

For the VAWT test case, the chord base Reynolds number is both dependent of the rotation speed and wind velocity. It is estimated that $\text{Re}_c$ is in the range of $90{,}000 < \text{Re}_c < 266{,}000$, which means that it is still in the range of validation.

**3.1 Airfoil Thickness.** We start by analyzing the effect of the airfoil thickness on the aerodynamic efficiency of the rotor. To this end, the turbulent flow on four NACA profiles (0006, 0010, 0015, and 0018) is computed. In this test case, the number of blades, the chord length, and the pitching axis location are fixed parameters, $N = 4$, $c = 0.25$ m, and $x'/c = 0.25$, respectively.

Figure 4(*a*) shows the variation of $C_P$ with $\lambda$ obtained for the different blade profiles. One can observe that, for this specific rotor dimensions, the power extraction with the NACA0006 and NACA0010 blades is significantly lower when compared with the thicker airfoils. However, as the airfoil thickness increases from 15% to 18% of the chord length, the increase in power coefficient



Downloaded From: http://solarenergyengineering.asmedigitalcollection.asme.org/ on 03/09/2016 Terms of Use: http://www.asme.org/about-asme/terms-of-use

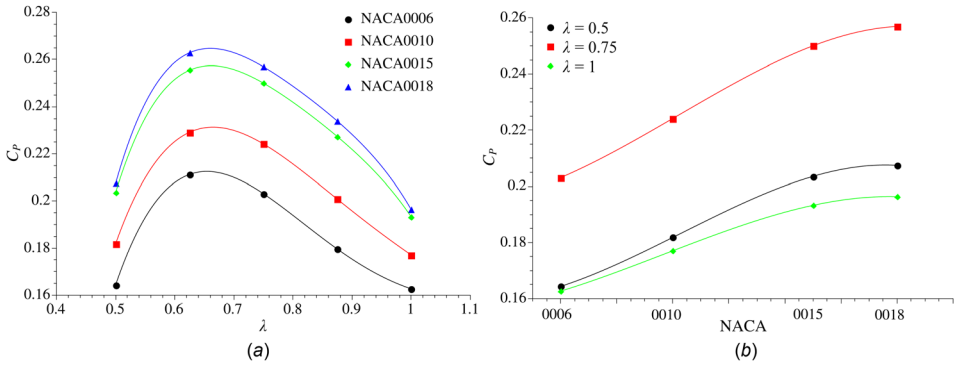


**Fig. 4 The results obtained for the airfoil thickness: (*a*) power coefficient variation with TSR and (*b*) power coefficient variation with airfoil thickness for different TSRs**

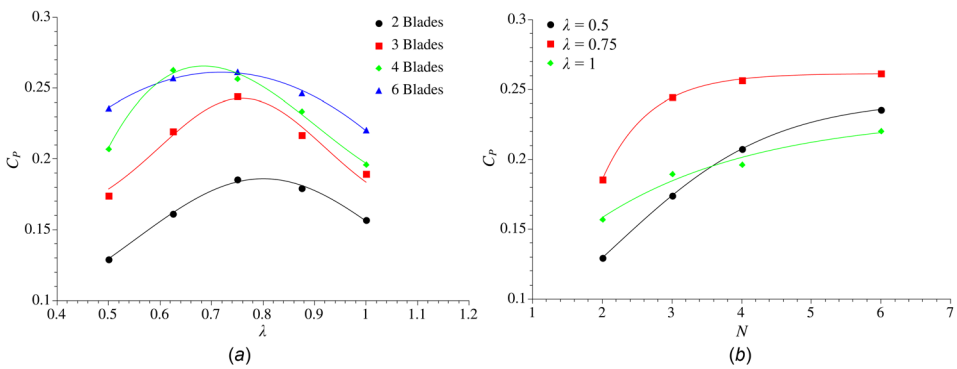


**Fig. 5 The results obtained for the variation of the number of blades: (*a*) power coefficient variation with TSR and (*b*) power coefficient variation with the number of blades for different TSRs**

is not so pronounced. This behavior is illustrated in Fig. 4(*b*), where $C_P$ is plotted as a function of the airfoil thickness, for constant values of $\lambda$. One can observe that the slope of the $C_P$ versus NACA is decreasing with the blade thickness and we can see that a maximum may have been reached for the NACA0018 profile.

**3.2 Number of Blades.** In the second test case, the only parameter that varies is the number of blades, $N$. Here, the NACA0018 airfoil was select, since it was the one that performed better in the thickness analysis. The chord length and the pitching axis location are again fixed at $c = 0.25\,\mathrm{m}$ and $x'/c = 0.25$, respectively. It is noted that, by increasing the number of blades, the rotor solidity

$$\sigma = \frac{N\,c}{R} \tag{8}$$

also increases. Equation (8) provides a parameter that measures the blade sweep area divided by the rotor frontal area. At this stage, it is important to define the criteria used to rank the configurations with respect to solidity. In the literature, it seems to exist a consensus that the limits of low solidity and high solidity are $\sigma = 0.1$ and $\sigma = 1$ [11]. Another possible effect that results from increasing $N$ is an increase of the aerodynamic interference effects, which could improve or decrease the aerodynamic performance of each blade.

Figure 5(*a*) shows the variation of $C_P$ with $\lambda$ computed in each one of the four rotors. One can observe that, for the lowest values of $\lambda$, the rotor that performs better is the one with six NACA0018 blades ($\sigma = 3$). In the range of $0.6 < \lambda < 0.8$, it is the rotor with four ($\sigma = 2$) blades that is capable of generating more torque. However, after $\lambda = 0.8$, the rotor with six blades is again preforming better, since the four-bladed rotor is showing a rapid decrease in torque production. The rotors with three ($\sigma = 1.5$) and two blades ($\sigma = 1$) are performing worst for all the cases. In Fig. 5(*b*), the variation of $C_P$ with the number of blades is plotted for constant values of $\lambda$. One can observe that, for low $\lambda$ values, the rotor seems to preform better as more blades are included. However, it seems that a maximum is reached with six blades.

**3.3 Chord-to-Radius Ratio.** The effect of solidity is now analyzed just by increasing the chord length and keeping the number of blades at a constant value of $N = 4$. For the remaining parameters, the values of Secs. 3.1 and 3.2 are used ($x'/c = 0.25$; NACA0018). By varying the chord length and keeping the radius constant, one also varies the chord-to-radius ratio. It is known that the $c/R$ ratio can have a strong influence in the turbine aerodynamics due to the flow curvature effects [17]. In curvilinear flow, the local angle of flow incidence and local velocity, along the blade chord line, are functions of radius, $R$, and chord location, ($x'$). This effect can be represented by a cambered airfoil in linear flow. In the VAWT of Fig. 1(*b*), the virtual camber is negative in the rotor top position ($\Psi = 90\,\mathrm{deg}$) and positive in the rotor bottom position ($\Psi = 270\,\mathrm{deg}$). The previous statement is only valid for high TSRs, where the velocity of the wind has a very small contribution in the relative velocity. The blade curvature effect is more pronounced in higher $c/R$; therefore, the length of the chord should play a significant role in the aerodynamic efficiency of the rotor.

Figure 6(*a*) shows the variation of $C_P$ with $\lambda$ for different chord lengths. For lower values of $C_P$, the rotor with larger blades ($c = 0.375\,\mathrm{m}$ and $\sigma = 3$) preforms better than the other two. This is mostly related to the fact that, at very low $\lambda$, the larger blades operate as more efficient drag devices. As the tip-speed velocity is



Downloaded From: http://solarenergyengineering.asmedigitalcollection.asme.org/ on 03/09/2016 Terms of Use: http://www.asme.org/about-asme/terms-of-use

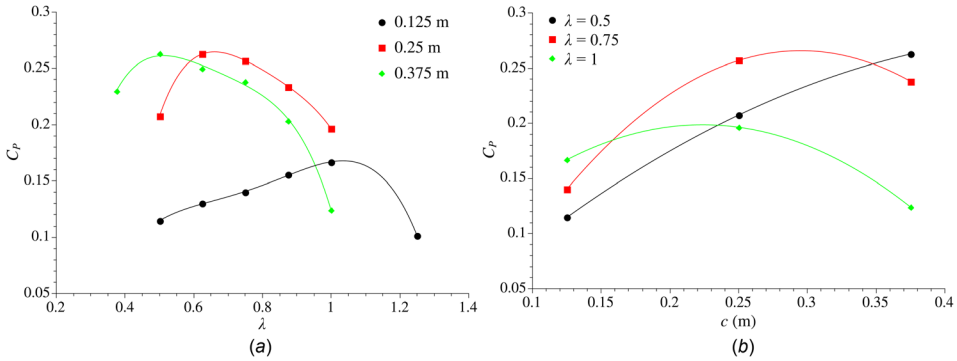


**Fig. 6 The results obtained for the variation of blade chord length: (*a*) power coefficient variation with TSR and (*b*) power coefficient variation with the blade chord length for different TSRs**

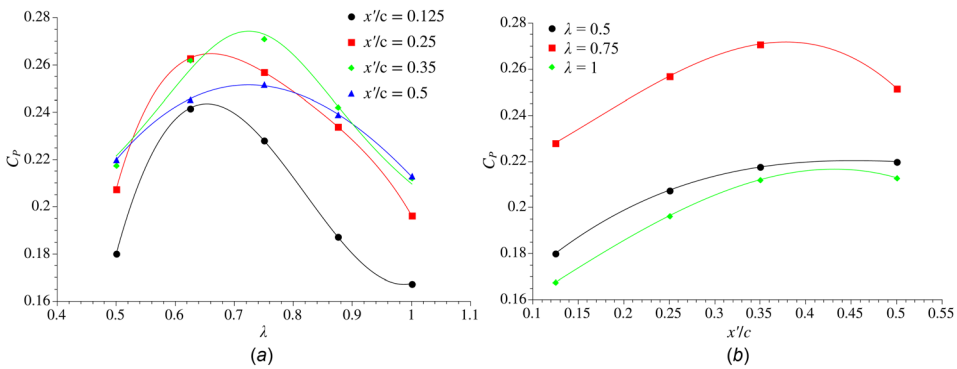


**Fig. 7 The results obtained for variation of the pitching axis location: (*a*) power coefficient variation with TSR and (*b*) power coefficient variation with the pitching axis location for different TSRs**

increased, the rotor should start operating as a lift-based device. In the range of $0.6 < \lambda < 1$, the intermediate airfoil ($c = 0.25$ m and $\sigma = 2$) preforms better. However, above $\lambda = 1$, the larger airfoils show a rapid decrease in $C_P$ in contradiction with the smallest airfoil ($c = 0.125$ m and $\sigma = 1$), where the maximum $C_P$ was computed between the values of $1 < \lambda < 1.1$. These results, together with the ones provided by the variation of the number of blades, clearly show that turbines with higher solidity preform better in very low $\lambda$ values, the same trend was observed in Ref. [30]. Figure 6(*b*) shows the variation of $C_P$ with the chord length for different values of $\lambda$. One can observe that for low TSRs, $\lambda = 0.5$, the power coefficient increases with the chord length. However, there should exist a limit for the chord length where the $C_P$ is maximum. For the $\lambda = 1$, the optimum blade, for this specific rotor dimension and pitch amplitude, should have a chord length in the range of $0.2 < c < 0.25$.

**3.4 Location of the Pitching Axis.** The location of the pitching axis in terms of $x'/c$ ratio is the last parameter to be analyzed. For this case, a chord length of $c = 0.25$ m was selected together with a total of four NACA0018 blades. The location of the pitching axis should ideally be determined by the location of the aerodynamic center. In Ref. [31], it was verified that the location of the aerodynamic center for a NACA0018 blade was at $x'/c = 0.285$. They have also demonstrated that this location is only valid until an angle of attack of 20 deg. Above that angle, the moment coefficient starts to increase and the location of the aerodynamic center starts to shift. In this section, we have analyzed a pitch amplitude of 30 deg. Such pitch amplitude does not mean that the actual angle of attack in all the azimuthal positions is higher than 20 deg; however, we will expect that this will occur in some specific locations. Therefore, different locations for the pitching axis were analyzed.

Figure 7(*a*) shows the variation of power coefficient with TSR. One can see that, for several values of $\lambda$, the $x'/c = 0.35$ is giving higher values of $C_P$. It is also observed that a more smooth distribution of $C_P$ is obtained when the pitching axis is located closer to half of chord length, $x'/c = 0.5$. In Fig. 7(*b*), we have again plotted the $C_P$ variation with the geometrical parameter, for constant values of $\lambda$. Here, it is possible to observe that for the lowest and intermediate value of $\lambda$, the optimum location of the pitching axis should be in the range of $0.35 < x'/c < 0.5$, and that this location is moved toward $x'/c = 0.5$ as we increase $\lambda$.

## 4 Comparison With a Fixed Pitch VAWT

In this section, the proposed design is compared with a conventional fixed pitch turbine. We assume that the optimized design is composed by a rotor with four NACA0018 blades with a pitching axis located at 35% of a chord length of $c = 0.25$ m. We have selected this design since it was the one that reached the highest $C_P$ value in the last "trial and error" parametric analysis. However, one can also verify that the six-bladed rotor is also very efficient for a wider range of $\lambda$.

Figure 8(*a*) shows a comparison between the fixed and variable pitch turbines in a $C_P$ versus $\lambda$ plot. Three pitch amplitudes are analyzed in the variable (V) and fixed (F) pitch rotors, namely, $\theta_0 = 5$ deg, 15 deg, and 30 deg. As expected, for the lowest $\lambda$, the $C_P$ increases with pitch amplitude, where the V-rotor with $\theta_0 = 30$ deg provides a $C_P$ four times superior to that provided by the F-rotors with $\theta_0 = 5$ deg and $\theta_0 = 15$ deg. One can also observe that the pitch amplitude must decrease as $\lambda$ increases. In particular, one can verify that the V-rotor with $\theta_0 = 15$ deg is quite



Downloaded From: http://solarenergyengineering.asmedigitalcollection.asme.org/ on 03/09/2016 Terms of Use: http://www.asme.org/about-asme/terms-of-use

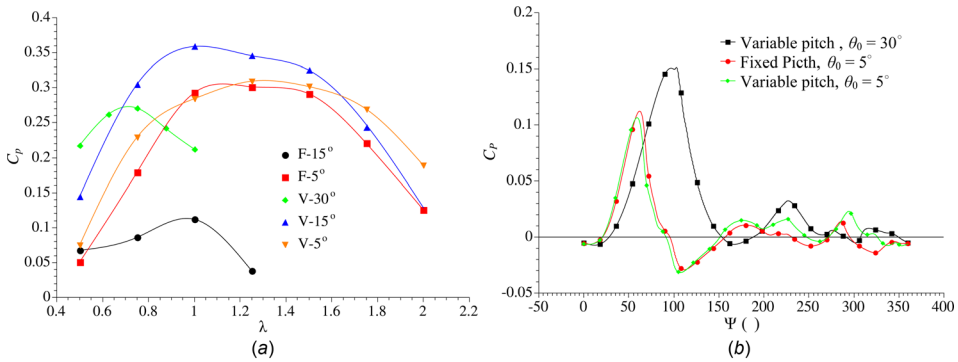


**Fig. 8 Comparison between the proposed and conventional design: (*a*) power coefficient variation with TSR (F—fixed pitch and V—variable pitch, for $\theta_0 = 5$ deg, 15 deg, and 30 deg) and (*b*) power coefficient variation with the azimuthal position of one blade for $\lambda = 0.5$**

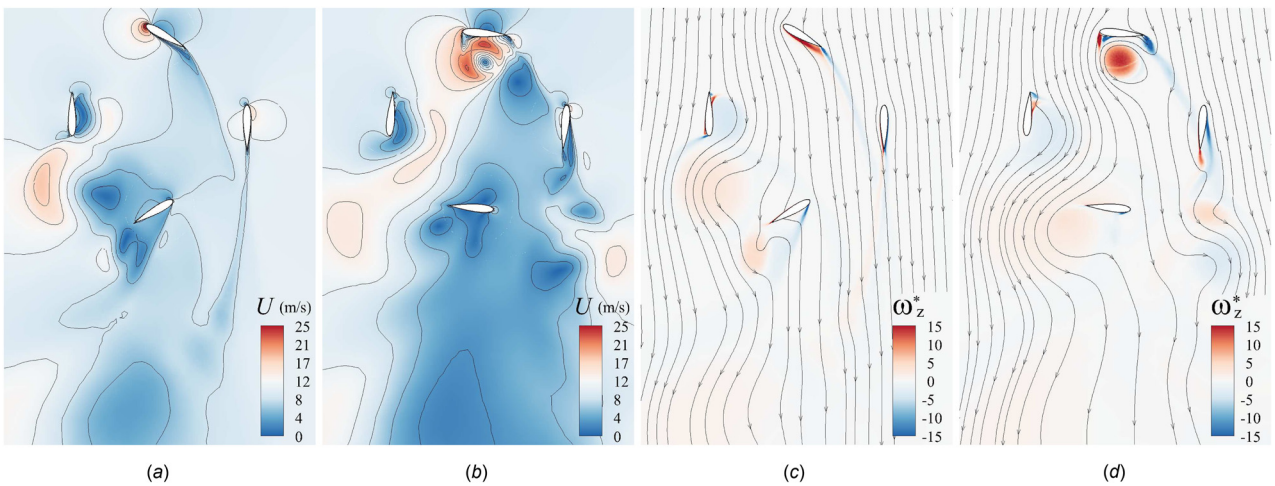


**Fig. 9 Instantaneous contour plots of velocity magnitude ($\lambda = 0.5$) computed after five revolutions in the (*a*) proposed design ($c = 0.25$ m; $N = 4$; NACA0018; $x'/c = 0.35$; and $\theta_0 = 30$ deg) and (*b*) conventional rotor with a fixed pitch of 5 deg. Instantaneous contour plots for the nondimensional vorticity, $\omega_z^* = \omega_z\, c/U_{\text{wind}}$, with super imposed streamlines: (*c*) proposed design and (*d*) conventional rotor.**

efficient in the range of $0.75 < \lambda < 1.5$ but if, for the same rotor, we decrease the amplitude into $\theta_0 = 5$ deg, more efficiency is obtained for $\lambda$ values above 1.75. For an amplitude of $\theta_0 = 5$ deg, the F-rotor gives a similar efficiency as the V-rotor in the $0.75 < \lambda < 1.5$ range, but it cannot provide the same torque in the remaining cases. The F-rotor with $\theta_0 = 15$ deg is here plotted to better illustrate the problems of VAWTs at low $\lambda$.

Figure 8(*b*) shows the variation of $C_P$ with the azimuthal position of a single blade in a fixed ($\theta_0 = 5$ deg) and in two variable ($\theta_0 = 30$ deg and $\theta_0 = 5$ deg) pitch rotors, for $\lambda = 0.5$. One can easily verify that a significant higher value of power is extracted with the V-rotor 30 deg blade, when this is in the frontal region of the rotor ($0\,\text{deg} < \Psi < 180\,\text{deg}$), and that some power is also obtained in the backward region ($180\,\text{deg} < \Psi < 360\,\text{deg}$). With a F-rotor, this is no longer possible: less power is extracted in the first two quadrants, and even some considerable negative torque is obtained in $90\,\text{deg} < \lambda < 160\,\text{deg}$, meaning that the turbine blade is providing energy to the flow. When the V-rotor 5 deg is compared with its fixed counterpart, a similar, although slightly lower, $C_p$ distribution is observed in the rotor frontal region. However, in the backward region, the V-rotor 5 deg preforms much better, since the critical angles of attack are being reduced by the pitching mechanism. These aspects are illustrated in Fig. 9, where the contour plots of velocity magnitude ((*a*) and (*b*)) and nondimensional vorticity, with superimposed stream lines ((*c*) and (*d*)), are shown. In these plots, one can observe that a more smooth flow is obtained with a variable pitch rotor, and that in the fixed pitch rotor a significant portion of kinetic energy is being converted into vorticity.

## 5 Conclusions

In this paper, we have proposed design guidelines for what could be the next generation of VAWTs. The proposed concept is based on a self-pitch turbine that prescribes a pitching schedule for the blades during the rotating cycle. We have demonstrated, through the use of numerical tools, that the proposed concept, when compared with a classical fix pitch VAWT, can generate higher torque for lower TSRs. Such increase for low and intermediate $\lambda$ is due to a reduction of the variation of the angle of attack, which reduces stall effects in several azimuthal positions of the rotor.

A parametric study was also performed for several key geometrical parameters ruling the design of variable pitch turbines. One could verify that the aerodynamic efficiency, at high pitch amplitudes, increases with airfoil thickness until a maximum is obtained for the NACA0018 blade. Regarding the number of blades, our results show that higher torque can be obtained at low $\lambda$ values with the six-bladed rotor, and that more blades seem to give a slightly constant torque production over a wider range of $\lambda$. The results for the chord-to-radius ratio show that higher torque is produced at a very low TSRs with larger blades and that the $c/R$



Downloaded From: http://solarenergyengineering.asmedigitalcollection.asme.org/ on 03/09/2016 Terms of Use: http://www.asme.org/about-asme/terms-of-use

should decrease with $\lambda$. The CFD solution for the pitching axis location shows that, for a given $\theta_0$, the optimum location is also dependent on $\lambda$, but should be located in the range $0.35 < x'/c < 0.5$.

For future work, several topics must be addressed:

(1) Explore the effect of the Reynolds number.
(2) Analyze the rotor behavior under realistic wind profiles.
(3) The definition of the optimum pitching schedule for the blades. This must be done in conjunction with the design of the mechanical system, since only structurally viable pitching kinematics is allowed, for the sake of integrity.
(4) Full three-dimensional analysis of the rotor in different operational conditions.
(5) Impact of the parasitic drag, associated with supporting arms and pitching mechanism, on the turbine efficiency.

## Acknowledgment

This work was performed as part of Project CROP, supported by the European Union within the 7th Framework Programme under Grant No. 323047 and also supported by C-MAST, Centre for Mechanical and Aerospace Sciences and Technologies, Research Unit No. 151.

## References

[1] Eriksson, S., Bernhoff, H., and Leijon, M., 2008, "Evaluation of Different Turbine Concepts for Wind Power," Renewable Sustainable Energy Rev., **12**(5), pp. 1419–1434.
[2] Pope, K., Dincer, I., and Naterer, G., 2010, "Energy and Exergy Efficiency Comparison of Horizontal and Vertical Axis Wind Turbines," Renewable Energy, **35**(9), pp. 2102–2113.
[3] Xisto, C. M., Pascoa, J. C., Leger, J., and Trancossi, M., 2014, "Wind Energy Production Using an Optimized Variable Pitch Vertical Axis Rotor," ASME Paper No. IMECE2014-38966.
[4] Benedict, M., Lakshminarayan, V., Pino, J., and Chopra, I., 2015, "Aerodynamics of a Small-Scale Vertical-Axis Wind Turbine With Dynamic Blade Pitching," AIAA J., (in press).
[5] Madsen, H., and Lundgren, K., 1980, *The Voith-Schneider Wind Turbine: Some Theoretical and Experimental Results on the Aerodynamics of the Voith-Schneider Wind Turbine*, Institute of Industrial Constructions and Energy Technology, Aalborg University Centre, Aalborg, Denmark.
[6] Pawsey, N. C. K., 2002, "Development and Evaluation of Passive Variable-Pitch Vertical Axis Wind Turbines," Ph.D. thesis, University of New South Wales, Sydney, NSW.
[7] Duquette, M. M., and Visser, K. D., 2003, "Numerical Implications of Solidity and Blade Number on Rotor Performance of Horizontal-Axis Wind Turbines," ASME J. Sol. Energy Eng., **125**(4), pp. 425–432.
[8] Mohamed, M., 2012, "Performance Investigation of H-Rotor Darrieus Turbine With New Airfoil Shapes," Energy, **47**(1), pp. 522–530.
[9] Roh, S.-C., and Kang, S.-H., 2013, "Effects of a Blade Profile, the Reynolds Number, and the Solidity on the Performance of a Straight Bladed Vertical Axis Wind Turbine," J. Mech. Sci. Technol., **27**(11), pp. 3299–3307.
[10] Chougule, P., and Nielsen, S., 2014, "Overview and Design of Self-Acting Pitch Control Mechanism for Vertical Axis Wind Turbine Using Multi Body Simulation Approach," J. Phys. Conf. Ser., **524**(1), p. 012055.
[11] Ahmadi-Baloutaki, M., Carriveau, R., and Ting, D. S.-K., 2014, "Straight-Bladed Vertical Axis Wind Turbine Rotor Design Guide Based on Aerodynamic Performance and Loading Analysis," Proc. Inst. Mech. Eng., Part A, **228**(7), pp. 742–759.
[12] Tjiu, W., Marnoto, T., Mat, S., Ruslan, M. H., and Sopian, K., 2015, "Darrieus Vertical Axis Wind Turbine for Power Generation I: Assessment of Darrieus {VAWT} Configurations," Renewable Energy, **75**, pp. 50–67.
[13] Leger, J. A., Páscoa, J. C., and Xisto, C. M., 2015, "Analytical Modeling of a Cyclorotor in Hovering State," Proc. Inst. Mech. Eng., Part G, **229**(12), pp. 2163–2177.
[14] Hwang, S., Min, Y., Lee, H., and Kim, J., 2008, "Development of a Four-Rotor Cyclocopter," J. Aircr., **45**(6), pp. 2151–2157.
[15] Benedict, M., 2010, "Fundamental Understanding of the Cycloidal-Rotor Concept for Micro Air Vehicle Applications," Ph.D. thesis, University of Maryland, College Park, MD.
[16] Benedict, M., Ramasamy, M., and Chopra, I., 2010, "Improving the Aerodynamic Performance of Micro-Air-Vehicle-Scale Cycloidal Rotor: An Experimental Approach," J. Aircr., **47**(4), pp. 1117–1125.
[17] Benedict, M., Jarugumilli, T., and Chopra, I., 2013, "Effect of Rotor Geometry and Blade Kinematics on Cycloidal Rotor Hover Performance," J. Aircr., **50**(5), pp. 1340–1352.
[18] Xisto, C. M., Páscoa, J. C., Leger, J. A., Masarati, P., Quaranta, G., Morandini, M., Gagnon, L., Schwaiger, M., and Wills, D., 2014, "Numerical Modelling of Geometrical Effects in the Performance of a Cycloidal Rotor," 11th World Conference on Computational Mechanics (WCCM XI), Barcelona, Spain, July 20-25, p. 1848.
[19] ANSYS, "ANSYS Fluent Theory Guide," ANSYS, Inc., Canonsburg, PA.
[20] Xisto, C. M., Páscoa, J. C., Abdollahzadeh, M., Leger, J. A., Schwaiger, M., and Wills, D., 2014, "PECyT—Plasma Enhanced Cycloidal Thruster," 50th AIAA/ASME/SAE/ASEE Joint Propulsion Conference, Cleveland, OH, July 28–30, AIAA Paper No. 2014-3854.
[21] Xisto, C. M., Pascoa, J. C., and Leger, J., 2014, "Cycloidal Rotor Propulsion System With Plasma Enhanced Aerodynamics," ASME Paper No. IMECE2014-38291.
[22] Gagnon, L., Quaranta, G., Morandini, M., Masarati, P., Lanz, M., Xisto, C. M., and Pascoa, J. C., 2014, "Aerodynamic and Aeroelastic Analysis of a Cycloidal Rotor," AIAA Paper No. 2014-2450.
[23] Trancossi, M., Dumas, A., Xisto, C. M., Páscoa, J. C., and Andrisani, A., 2014, "Roto-Cycloid Propelled Airship Dimensioning and Energetic Equilibrium," SAE Paper No. 2014-01-2107.
[24] Hansen, M. O., and Sørerensen, D. N., 2001, "CFD Model for Vertical Axis Wind Turbine," European Wind Energy Conference and Exhibition (EWEC '01), Copenhagen, Denmark, July 2–7.
[25] Edwards, J. M., Angelo Danao, L., and Howell, R. J., 2012, "Novel Experimental Power Curve Determination and Computational Methods for the Performance Analysis of Vertical Axis Wind Turbines," ASME J. Sol. Energy Eng., **134**(3), p. 031008.
[26] Ferreira, C. J. S., Bijl, H., van Bussel, G., and van Kuik, G., 2007, "Simulating Dynamic Stall in a 2D VAWT: Modeling Strategy, Verification and Validation With Particle Image Velocimetry Data," J. Phys. Conf. Ser., **75**(1), p. 012023.
[27] Ferreira, C. J. S. A., van Zuijlen, A., Bijl, H., van Bussel, G., and van Kuik, G., 2010, "Simulating Dynamic Stall in a Two-Dimensional Vertical-Axis Wind Turbine: Verification and Validation With Particle Image Velocimetry Data," Wind Energy, **13**(1), pp. 1–17.
[28] Ferreira, C. J. S. A., van Bussel, G. J. W., van Kuik, G. A. M., and Scarano, F., 2011, "On the Use of Velocity Data for Load Estimation of a VAWT in Dynamic Stall," ASME J. Sol. Energy Eng., **133**(1), p. 011006.
[29] Spalart, P. R., and Rumsey, C. L., 2007, "Effective Inflow Conditions for Turbulence Models in Aerodynamic Calculations," AIAA J., **45**(10), pp. 2544–2553.
[30] Sanyer, W., 2011, "The Development of a Wind Turbine for Residential Use," Master's thesis, North Carolina State University, Raleigh, NC.
[31] Goett, H. J., and Bullivant, W. K., 1938, "Tests of NAC A 0009, 0012, and 0018 Airfoils in the Full-Scale Tunnel," National Advisory Committee for Aeronautics, Washington, DC, NACA Technical Report No. 647.



**Downloaded From: http://solarenergyengineering.asmedigitalcollection.asme.org/ on 03/09/2016 Terms of Use: http://www.asme.org/about-asme/terms-of-use**